JACS
JOURNAL OF THE AMERICAN CHEMICAL SOCIETY

Article

pubs.acs.org/JACS

Lanthanide Cofactors Accelerate DNA-Catalyzed Synthesis of Branched RNA

Fatemeh Javadi-Zarnaghi and Claudia Höbartner*

Research Group Nucleic Acid Chemistry, Max Planck Institute for Biophysical Chemistry, Am Fassberg 11, 37077 Göttingen, Germany

Supporting Information

ABSTRACT: Most deoxyribozymes (DNA catalysts) require metal ions as cofactors for catalytic activity, with Mg^{2+}, Mn^{2+}, and Zn^{2+} being the most represented activators. Trivalent transition-metal ions have been less frequently considered. Rare earth ions offer attractive properties for studying metal ion binding by biochemical and spectroscopic methods. Here we report the effect of lanthanide cofactors, in particular terbium (Tb^{3+}), for DNA-catalyzed synthesis of 2′,5′-branched RNA. We found up to 10^4-fold increased ligation rates for the 9F7 deoxribozyme using 100 μM Tb^{3+} and 7 mM Mg^{2+}, compared to performing the reaction with 7 mM Mg^{2+} alone. Combinatorial mutation interference analysis (CoMA) was used to identify nucleotides in the catalytic region of 9F7 that are essential for ligation activity with different metal ion combinations. A minimized version of the DNA enzyme sustained high levels of Tb^{3+}-assisted activity. Sensitized luminescence of Tb^{3+} bound to DNA in combination with DMS probing and DNase I footprinting results supported the CoMA data. The accelerating effect of Tb^{3+} was confirmed for related RNA-ligating deoxyribozymes, pointing toward favorable activation of internal 2′-OH nucleophiles. The results of this study offer fundamental insights into nucleotide requirements for DNA-catalyzed RNA ligation and will be beneficial for practical applications that utilize 2′,5′-branched RNA.

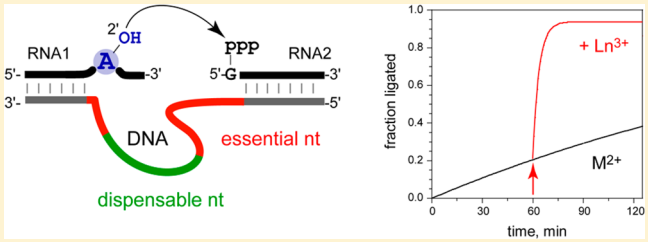

INTRODUCTION

Deoxyribozymes (DNA enzymes) are catalytically active synthetic DNAs that are of interest in fundamental research and have found practical use as components of biosensors and functional devices in DNA nanotechnology.[1−3] In the field of nucleic acids research, DNA enzymes are established catalysts for preparative applications, including the site-specific cleavage and ligation of RNA substrates.[3−5] Several deoxyribozymes have been described that enable the efficient synthesis of 2′,5′-branched RNA,[6] a class of nucleic acid structures related to lariat RNA, which is produced during RNA splicing by the group II intron and the spliceosome. DNA enzymes that synthesize 2′,5′-branched RNA activate the 2′-hydroxyl group of the branch-site nucleotide in the acceptor strand for the nucleophilic attack onto the 5′-triphosphate of the donor RNA (Figure 1a).[6] Upon release of pyrophosphate as the leaving group, a new 2′,5′-phosphodiester bond between donor and acceptor is formed. For this reaction to occur, the RNA substrates hybridize to the binding arms of the deoxyribozymes, and form active RNA−DNA complexes in different topologies. In the 7S11 DNA enzyme family,[7] the branch-site nucleotide is selected by Watson−Crick base pairing directly upstream and downstream of the reaction site and is located in the center of a three-helix junction architecture.[8] In the 9F7 DNA enzyme family,[9] the branch-site nucleotide is recognized in an as-yet unknown structural context, in which the nucleotides 3′ of the branch site are not part of a standard double helix, but their interaction partners in the deoxyribozyme core have not yet been identified.[10]

The 9F7 deoxyribozyme (Figure 1a) was identified by in vitro selection from a DNA pool containing 40 random nucleotides[9] and has been well characterized with respect to substrate scope.[10] However, at the outset of this study it was not known which of the 40 nucleotides in the catalytic region are essential for formation of the active site and are potentially involved in the catalytic mechanism. Based on secondary structure predictions, the presence of a stem-loop structure in the core region of 9F7 is conceivable.[6] It can be expected that several of the nucleotides in the large stem-loop and the upstream single-stranded region participate in tertiary structure formation and may play crucial roles in catalysis.

In contrast to nucleolytic ribozymes and RNA-cleaving deoxyribozymes, the catalytic mechanisms of RNA-ligating DNA enzymes have not been studied in detail. Like most nucleic acid catalysts, deoxyribozymes that synthesize 2′,5′-branched RNA use divalent metal ions, such as Mg^{2+}, Mn^{2+}, or Zn^{2+} as cofactors for efficient catalysis. It is poorly understood how metal ions and/or nucleobases interact with the substrates along the reaction coordinate, which involves in-line attack of the 2′-OH group on the α phosphate and release of pyrophosphate. In analogy to ribozyme mechanisms, the

Received: June 19, 2013
Published: July 28, 2013

   dx.doi.org/10.1021/ja406162z | J. Am. Chem. Soc. 2013, 135, 12839−12848

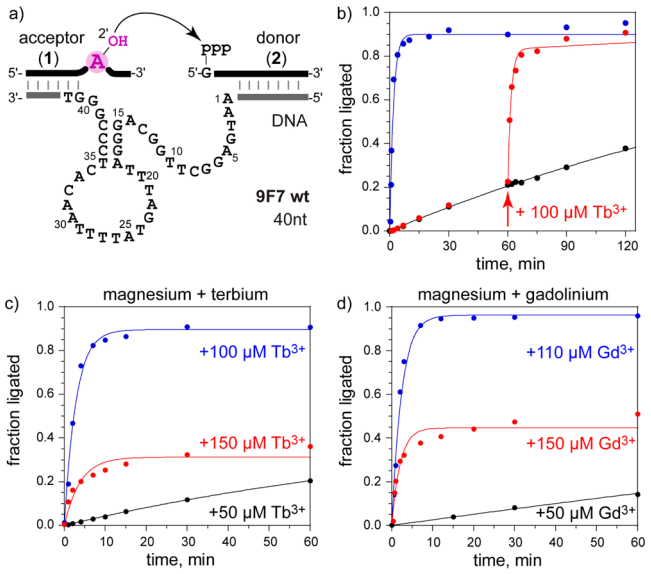

Figure 1. (a) Original 9F7 deoxyribozyme[9] that catalyzes the nucleophilic attack of the 2′-OH group of the branch-site adenosine (of acceptor RNA **1**) into the 5′-triphosphate of the donor RNA **2**. (b) Acceleration of ligation by Tb^{3+}; black: 80 mM Mg^{2+}, k_{obs} = 0.003 min^{-1}; blue: 80 mM Mg^{2+} + 100 μM Tb^{3+}, k_{obs} = 0.35 min^{-1}; red: chase experiment with addition of Tb^{3+} after 60 min ligation with 80 mM Mg^{2+}. (c, d) Time course of ligation at three different lanthanide concentrations in presence of 80 mM Mg^{2+}: (c) Tb^{3+} (μM), k_{obs} (min^{-1}); black: 50, 0.009; blue: 100, 0.35; red: 150, 0.26; (d) Gd^{3+} (μM), k_{obs} (min^{-1}); black: 50, 0.002; blue: 110, 0.41; red: 150, ~0.5.

reaction partners and the transition state are likely candidates for metal coordination. In addition, metal ions can also play essential roles outside of the catalytic core via stabilization of critical tertiary structure elements.[11]

Several methods are available to study metal ion interactions and to delineate critical nucleobase contacts in nucleic acid enzymes.[12] Lanthanide ions have proven useful for probing metal ion binding in ribozymes.[13] The high affinity to Mg^{2+} binding sites and the similar pK_a of hydrated Ln^{3+} ions compared to Mg^{2+} make rare earth ions good candidates for biochemical probing experiments, such as Tb^{3+} footprinting.[14] Moreover, the useful luminescent properties of lanthanides, such as Tb^{3+} and Eu^{3+}, have been harnessed in studies of metal ion binding to RNA.[15−17] Tb^{3+} has been found to inhibit RNA cleavage by the small nucleolytic ribozymes, including the hammerhead and hairpin RNA enzymes.[14,18] The effect of lanthanides on the activity of artificial RNA-cleaving ribozymes and deoxyribozymes has also been investigated. The first known deoxyribozyme, a lead-dependent phosphodiester-cleaving DNA[19] showed activity with the small Lu^{3+} ion as the sole metal ion.[20] A related ribozyme, the leadzyme,[21] was activated when rare earth ions (in particular Nd^{3+}) were present in addition to Pb^{2+}.[22] In contrast, the RNA-cleaving 8−17 deoxyriboyzme[23] was strongly inhibited by Tb^{3+}.[24] Recently, lanthanides have been reported as cofactors for DNA-catalyzed hydrolysis of DNA.[25] In this case, Ce^{3+}, Eu^{3+}, or Yb^{3+} were included with Zn^{2+} as cofactors during in vitro selection and were found to be required for activity of the isolated deoxyribozymes.

Besides achieving a better understanding of the mechanism of DNA-catalyzed RNA ligation, one of our research goals is to develop DNA enzymes for practical utility. Successful engineering of DNA catalysts requires knowledge of structural and functional principles of deoxyribozymes. In this respect, we explore DNA catalysts that have proven useful for the manipulation of RNA, such as linear ligation, branched ligation, and site-specific modification. We have developed combinatorial probing methods to identify nucleotides and to pinpoint the essential functional groups that are required for catalytic activity.[26,27] Here, we report on functional studies of 2′,5′-branched RNA-forming deoxyribozymes and discuss the interesting finding of lanthanide-mediated acceleration of DNA-catalyzed RNA ligation by 9F7 and related DNA enzymes. We focus on Tb^{3+} due to its particular properties as a structural probing agent and promising candidate for spectroscopic studies, and we demonstrate that several other lanthanides have similar accelerating effects on 9F7 catalysis. We employed combinatorial mutation interference analysis (CoMA)[26] under various conditions to identify functional nucleotides, devised an efficient minimized version of the DNA, and examined metal ion binding and DNA folding by luminescence and footprinting experiments.

RESULTS AND DISCUSSION

Metal Ion Cofactors for 9F7 DNA-Catalyzed RNA Ligation. The 9F7 deoxyribozyme (Figure 1a) was identified together with related active DNA sequences by in vitro selection, using Mg^{2+} as cofactor for RNA ligation.[9] The DNA-catalyzed synthesis of 2′,5′-branched RNA with 9F7 occurred with a rather slow ligation rate of 0.003 min^{-1} with 80 mM Mg^{2+} at pH 7.5 and 37 °C. We were intrigued by our unexpected observation that the addition of Tb^{3+} at μM concentrations impressively accelerated the DNA-catalyzed ligation reaction. In the presence of 100 μM Tb^{3+} and 80 mM Mg^{2+}, the k_{obs} reached 0.35 min^{-1}, which was ca. 120-fold faster than in the absence of Tb^{3+}. In a chase experiment, Tb^{3+} was added to the reaction mixture to a final concentration of 100 μM after 60 min of ligation with only Mg^{2+} (Figure 1b), demonstrating that the acceleration of product formation was caused by Tb^{3+}.

Earlier reports demonstrated considerably faster ligation rates for 9F7 using Mn^{2+} instead of Mg^{2+} as divalent metal ion cofactor.[9,10] At 20 mM Mn^{2+}, k_{obs} reached 0.3 min^{-1}, but a 10-fold reduced [Mn^{2+}] of 2 mM supported only similar ligation rates as 80 mM Mg^{2+} (Figure S1). Addition of Tb^{3+} to Mn^{2+}-mediated reactions resulted in 5−500-fold faster ligation rates than in the absence of Tb^{3+} (see below).

Variation of metal ion conditions for ribozyme-catalyzed reactions can potentially activate or repress alternative reaction sites.[28] Therefore, the ligation products generated by 9F7 under various metal ion conditions were investigated for homogeneity. Alkaline hydrolysis of isolated branched RNAs confirmed that the presence of Tb^{3+} did not change the site of reaction (data not shown).

The finding of Tb^{3+}-mediated acceleration of the 9F7-catalyzed RNA ligation reaction is significant, particularly in the context of earlier studies of lanthanide effects on ribozyme and deoxyribozyme activities that reported inhibition of catalysis.[14,24] Only under special conditions, small acceleration effects were found for nucleolytic ribozymes. For example, when tested in the presence of high concentrations of Na^{+} or spermidine (>1 M), low amounts of Tb^{3+} (<25 μM) accelerated the hairpin ribozyme-catalyzed RNA cleavage up to 2.5-fold, while higher Tb^{3+} (>30 μM) inhibited the ribozyme.[14] With an optimal combination of Nd^{3+} and Pb^{2+}, the leadzyme catalyzed RNA cleavage about 20-fold faster than

dx.doi.org/10.1021/ja406162z | J. Am. Chem. Soc. 2013, 135, 12839−12848

with Pb^{2+} alone.[22] The effects for the 9F7 deoxyribozyme are much larger, but rate and yield of the ligation are also strongly dependent on the Tb^{3+} concentration. While 100 μM Tb^{3+} activated the DNA enzyme 120-fold in combination with 80 mM Mg^{2+}, 50 μM Tb^{3+} led to almost no acceleration, and a higher concentration of 150 μM Tb^{3+} caused fast reaction of only a fraction of the available RNA substrate, resulting in a reduced amplitude with retained high rate constant (Figure 1c). Comparable effects were observed for Eu^{3+} and Gd^{3+} (Figures 1d and S2), which have similar ionic radii (1.04–1.07 Å) and pK_a values (7.8–8.0) of bound water molecules compared to Tb^{3+}.[29] Early lanthanide ions (La^{3+} and Ce^{3+}) also accelerated the DNA-catalyzed ligation efficiently, but the effect was less pronounced with Yb^{3+}, which is the last f-block element in the lanthanide row (Figure S2). Other trivalent nonlanthanide metal ions neither accelerated nor inhibited 9F7-catalyzed RNA ligation (Al^{3+} or Fe^{3+} were tested up to 100 μM in presence of 80 mM Mg^{2+}).

A more detailed analysis of the concentration-dependent lanthanide effect is depicted in Figure 2. Plotting the yield of

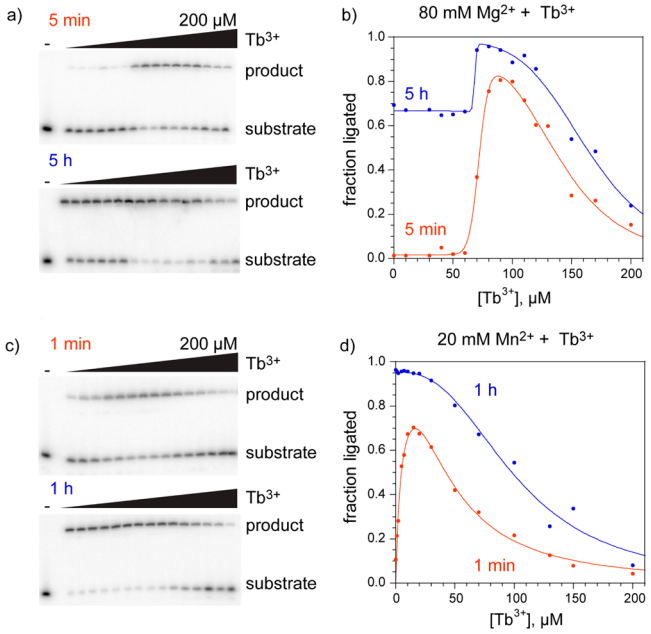

Figure 2. (a) Ligation yield at different [Tb^{3+}] with 80 mM Mg^{2+}. Gel images show yield after 5 min (top) and 5 h (bottom) reaction at 37 °C. (b) Plot of data in (a) shows optimal Tb^{3+} concentration at 100 μM. (c) Gel image of terbium titration; ligation yields at 1 min (top) and 1 h (bottom) reaction time in presence of 20 mM Mn^{2+}. (d) Plot of data in (c) shows optimal Tb^{3+} concentration at 10–20 μM. For curve fit description see Supporting Information (analogous plots for Eu^{3+} and Gd^{3+} are in Figure S3).

ligated RNA product as a function of [Tb^{3+}], in the presence of either 80 mM Mg^{2+} (Figure 2b) or 20 mM Mn^{2+} (Figure 2d), revealed the optimum concentration. With Mg^{2+}, the addition of Tb^{3+} had no effect up to a "critical" concentration of ca. 50 μM. The activity of the deoxyribozyme strongly increased up to the optimal concentration of 100 μM Tb^{3+}, at which ~80% ligation product was formed within 5 min. Further increase in [Tb^{3+}] up to 200 μM caused reduced ligation yields, which dropped significantly below those achievable in the absence of Tb^{3+}. With Mn^{2+}, the optimal [Tb^{3+}] was ca. 10-fold lower than with Mg^{2+}, which was best visible at early time points (e.g., after 1 min). When Tb^{3+} was tested as the only cofactor for 9F7 (at 10–100 μM Tb^{3+}), i.e., in the absence of Mn^{2+} or Mg^{2+}, no ligation was observed up to 24 h. In fact, substantial degradation of the RNA substrate was observed above 70 μM Tb^{3+} (when no divalent metal ions were present). Increasing the concentration of monovalent ions from 150 mM Na^+ and 2 mM K^+ up to 3 M Na^+ or 2 M K^+ (again in the absence of divalent metal ions) eliminated Tb^{3+}-mediated hydrolysis but did not support 9F7 catalysis.

The presence of optimal concentrations of Tb^{3+} increased the affinity for the divalent metal ions (Figure 3). The $K_{d,app}$ for

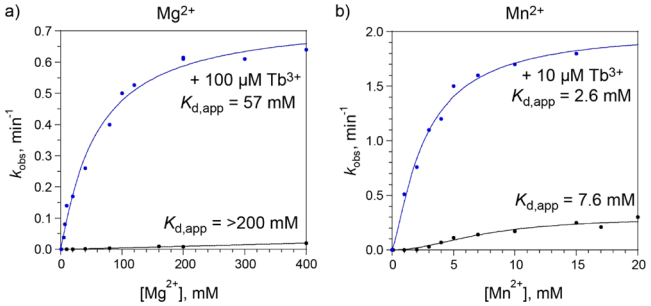

Figure 3. Dependence of ligation activity on divalent metal ion concentration in absence (black) and presence (blue) of optimal Tb^{3+} concentration: (a) Mg^{2+} titration, with or without 100 μM Tb^{3+}; (b) Mn^{2+} titration, with or without 10 μM Tb^{3+}. Plots of ligation rate k_{obs} (min^{-1}) versus [M^{2+}] (mM); fit equation: $k_{obs} = k_{max}*[M^{2+}]/(K_{d,app} + [M^{2+}])$.

Mg^{2+} decreased from >200 to 57 mM, and $K_{d,app}$ for Mn^{2+} decreased ca. 3-fold from 7.6 to 2.6 mM. The impressive effect of Tb^{3+} is especially visible at low divalent metal ion concentrations. At 2 mM Mn^{2+}, addition of 10 μM Tb^{3+} caused almost 500-fold acceleration. The lowest [Mg^{2+}], which led to detectable ligation product (1%) after 24 h, was 7 mM Mg^{2+}. Addition of 100 μM Tb^{3+} to 7 mM Mg^{2+} caused 10^4-fold faster ligation to yield >95% product in 1 h, thereby reducing $t_{1/2}$ from 1600 h to 10 min (Table 1).

Table 1. Acceleration of 9F7-Catalyzed RNA Ligation by Tb^{3+} in Presence of Mg^{2+}

[Mg^{2+}] mM	[Tb^{3+}] μM	k_{obs} min^{-1}	ligation yield	$t_{1/2}$	acceleration by Tb^{3+}
7	–	7×10^{-6}	1% in 24 h	~1600 h	
7	100	0.08	>95% in 1 h	~10 min	~10 000-fold
10	–	3×10^{-5}	1% in 5.5 h	~400 h	
10	100	0.14	>95% in 0.5 h	~5 min	~5 000-fold
80	–	0.003	>95% in 16 h	~4 h	
80	100	0.35	>95% in 0.15 h	~2 min	~120-fold

All kinetic assays of the ligation reactions were performed in 50 mM HEPES buffer pH 7.5, with 150 mM NaCl and 2 mM KCl. Addition of up to 100 μM trivalent ions did not significantly influence the ionic strength of the solution in comparison to the same divalent metal ion concentration in the absence of Tb^{3+}. Therefore the effect of Tb^{3+}-mediated acceleration is not easily explained by changes in ionic strength that could lead to stabilization of the preligation complex. In contrast, more specific interactions must be responsible for the

dx.doi.org/10.1021/ja406162z | J. Am. Chem. Soc. 2013, 135, 12839–12848

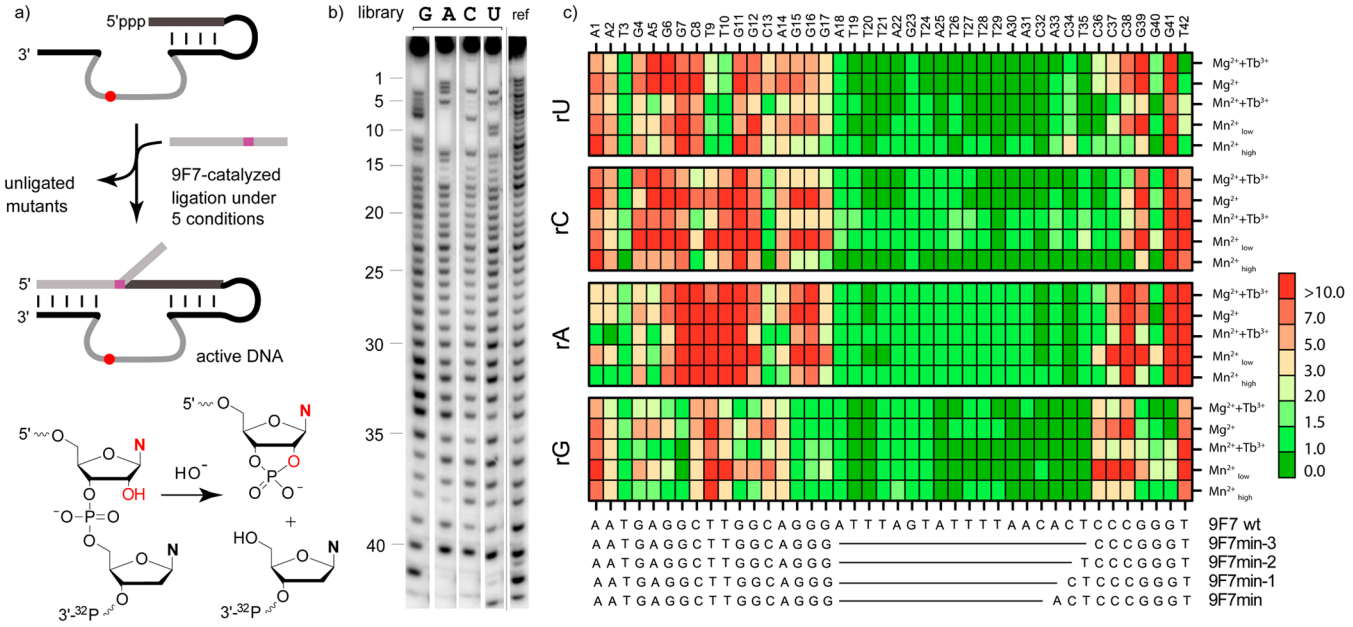

Figure 4. Combinatorial mutation interference analysis of 9F7; four mutant libraries (corresponding to one of the four standard ribonucleotides statistically distributed in the DNA) were analyzed under five different conditions: Mn^{2+} high (20 mM), Mn^{2+} low (2 mM), Mn^{2+} (2 mM) + Tb^{3+} (10 μM), Mg^{2+} (80 mM), and Mg^{2+} (80 mM) + Tb^{3+} (100 μM). (a) Schematic depiction of library separation and alkaline hydrolysis. (b) Representative hydrolysis gels of active fractions (separation after ligation reaction with 20 mM Mn^{2+}) and unseparated reference lane (full gel images and interference values are in Figure S8). (c) Contour plot of interference values for all four libraries under five conditions; minimized 9F7 variants are given below the graph.

observed effects. A likely candidate for metal ion interaction in the ligation reaction is the triphosphate of the donor RNA. Hydroxo complexes of transition-metal ions are known to accelerate the hydrolysis of activated phosphate esters,[30] as, for example, the triphosphate of ATP.[31] It is conceivable that the synergistic effect of M^{2+} and Tb^{3+} is related to increased electrophilicity of the α phosphate in RNA **2** upon metal ion coordination. The reduced ligation amplitude could potentially be rationalized by accelerated competing hydrolysis of the triphosphate at higher Tb^{3+} concentrations. This hypothesis was tested by HPLC analysis of the fate of donor RNA upon incubation under different metal ion combinations but was not substantiated by our experimental results. RNA **2** was hybridized to a complementary DNA oligonucleotide resembling the deoxyribozyme binding arm and was incubated under various conditions. More than 80% of triphosphate was still intact after 1 h in presence of 100 μM Tb^{3+} and 80 mM Mg^{2+}; the triphosphate content decreased only slightly with 200 μM Tb^{3+} (Figure S4). In contrast, the ligation yield was strongly reduced to 30% with 200 μM Tb^{3+} (compared to 89% yield with 100 μM Tb^{3+}), although the donor substrate **2** was supplied in 6-fold excess over acceptor RNA **1**. These results indicated that the competing triphosphate hydrolysis was not responsible for the reduced ligation amplitude, but higher Tb^{3+} likely caused misfolding of the deoxyribozyme into an inactive conformation. When the donor, acceptor, and deoxyribozyme were used in equimolar ratio for preparative purpose, the DNA-catalyzed RNA ligation reaction was also accelerated by Tb^{3+}. To maintain good yield after short incubation times, the RNA/DNA concentration was 1 μM, resulting in 100 equiv Tb^{3+} with respect to preligation complex. At higher RNA/DNA concentration (lower Tb^{3+} to nucleic acid ratio), the ligation reaction was slower (Figure S5), likely due to increased unspecific binding of Tb^{3+} to the nucleic acids, causing reduced availability of "active" Tb^{3+} ions.

To further explore the specific synergistic effects of divalent Mg^{2+}/Mn^{2+} ions and trivalent rare earth ions on activation of the RNA substrates for 9F7-catalyzed ligation, we investigated phosphorothioate-modified donor substrates in which one oxygen atom at either the α or γ phosphate was replaced by sulfur. Phosphorothioate (PS) interference and metal ion rescue experiments have the potential to reveal crucial information about metal ion interactions in the active site.[32] Installation of γ-PS can be easily achieved by in vitro transcription using γ-*S*-GTP. In contrast, transcription with α-*S*-GTP results in incorporation of PS at the 5′-terminal α-phosphate and at all other guanosines in the strand. To avoid cumulative effects of more than one PS in the substrate, we designed an alternative donor substrate (**2a**), that contained only one guanosine at the 5′-end and otherwise consisted of only A, C, and U (sequences in Table S1).

Replacement of the γ-phosphate by PS in RNA **2** caused a considerably reduced ligation rate, which was about 100-fold slower than for wt RNA **2** (in presence of 80 mM Mg^{2+}; 15-fold slower in presence of 20 mM Mn^{2+}, Figure S6), but addition of Tb^{3+} did not change the outcome of the reaction. These results indicated that the larger and softer sulfur atom was less accommodated than oxygen at the γ position and lent support to the hypothesis of preferred interaction of the terminal phosphate with hard lanthanides. Softer and more thiophilic metal ions, such as Cd^{2+} and Mn^{2+}, could potentially rescue PS effects. Addition of 1 mM Cd^{2+} did not significantly improve the ligation rate (Figure S6c), while addition of 2 mM Mn^{2+} accelerated ligations of both PO and PS RNAs by a factor of ca. 10−20, which indicated no specific rescue effect for the γ PS (Figure S6a). In the presence of higher Mn^{2+} concentration (20 mM Mn^{2+} with 80 mM Mg^{2+}), the ligation of the PS substrate

dx.doi.org/10.1021/ja406162z | J. Am. Chem. Soc. 2013, 135, 12839−12848

was accelerated 250-fold, while the reaction of the PO substrate was only ca. 70-fold faster than with Mg^{2+} alone.

The alternative substrate **2a** was ligated less efficiently than **2** under the standard reaction conditions (k_{obs} ca. 10-fold slower). Replacement of the α phosphate with PS resulted in comparable ligation rates using Mn^{2+} as cofactor, while PS at the γ position again severely inhibited the reaction (Figure S7). Upon addition of 1 mM Cd^{2+}, the k_{obs} for the α-PS analog of **2a** increased ca. 3-fold, while the ligation rate of the unmodified substrate remained unaffected (Figure S7a). Presence of 10 μM Tb^{3+} had a comparable 3-fold effect for the α-PS substrate, while ligation of the unmodified RNA **2a** was ca. 10-fold faster than in the absence of Tb^{3+} (Figure S7b). Collectively, these results point toward important interactions at the α- and γ-phosphates of the donor RNA, although the PS and rescue effects were less pronounced than for other metalloribozymes.[33,34]

Combinatorial Mutation Interference Analysis. Besides the nucleophile and electrophile involved in the reaction, nucleotides of the catalytic core are also likely to participate in metal ion interactions. Therefore, we investigated if all 40 nucleotides of the original 9F7 core region were necessary for catalysis and if any candidate nucleotides were responsive to different metal ions.

We capitalized on our recently developed approach for combinatorial mutation interference analysis (CoMA)[26] to further examine the 9F7 deoxyribozyme. In this method, four combinatorial DNA libraries are prepared by solid-phase synthesis, using mixtures of phosphoramidites that yield on average one mutation per DNA molecule, statistically distributed over the length of the DNA of interest. Incorporation of mutations as ribonucleotides enables analysis of interference effects by alkaline hydrolysis followed by denaturing PAGE analysis. A separate library is synthesized with each of the four standard ribonucleotides. A key step in the analysis is the separation of active from inactive library members. The DNA-catalyzed ligation reaction is performed in a bimolecular format, with the donor substrate covalently attached to the DNA library (Figure 4a). Upon incubation with the acceptor RNA under desired reaction conditions, only those library variants yield ligation products, in which the mutations do not interfere with catalysis. On the sequencing gels for analysis, the detrimental mutations are identified as missing bands (Figure 4b). Interference effects are quantified as the ratio of band intensities in the active fraction and the unseparated reference library and clearly distinguish essential from mutable nucleotides.

Here, CoMA was performed for 9F7 under five different ligation conditions. To compare nucleotide requirements of 9F7 at low and high bivalent metal ion concentrations, we chose 2 mM Mn^{2+}, 20 mM Mn^{2+}, and 80 mM Mg^{2+}. To examine the influence of Tb^{3+}, we also included the analysis in the presence of 10 μM Tb^{3+} with 2 mM Mn^{2+} as well as 100 μM Tb^{3+} with 80 mM Mg^{2+} (note that 10 and 100 μM Tb^{3+} were the optimum concentrations in presence of Mn^{2+} and Mg^{2+}, respectively). The different ligation kinetics observed under these different metal ion conditions were taken into account for the ligation reaction before the separation step. Too short incubation times would exclude the slow mutants present in the library and therefore increase the interference values for positions where mutations reduce the ribozyme activity but are not detrimental. On the other hand, too long incubation would enrich very slow mutants in the ligated fraction, and therefore the mutation effects could be hidden in the bulk of low interference values. We chose the reaction times according to the results of the trimolecular 9F7 ligation kinetics in the respective conditions, i.e., reaction times that yield ~90% of the maximum yield (that is, 10 h with 2 mM Mn^{2+}, 8 h with 80 mM Mg^{2+}, 2 h with 100 μM Tb^{3+} + 80 mM Mg^{2+}, 1 h with 10 μM Tb^{3+} + 2 mM Mn^{2+}, and 20 min with 20 mM Mn^{2+}). For all five reactions, these incubation times reproducibly resulted in formation of ca. 30% ligation product (i.e., ca. one-third of the library was in the active fraction). Figure 4b shows a representative hydrolysis gel for the active fractions of all four libraries (after ligation with 20 mM Mn^{2+}) in comparison with an unseparated reference lane. The full gel images for all five conditions are shown in Figure S8. The interference values were calculated and plotted in the contour plot in Figure 4c; green indicates low interference (i.e., the mutation is tolerated), and red indicates strong interference, (i.e., the mutation inhibits catalytic activity).

The most striking result from this analysis is the large green region between nucleotides 18 and 35 where all mutations are tolerated under all tested conditions, suggesting that this stretch of nucleotides does not play any essential role in catalysis. All 18 nucleotides could indeed be removed, resulting in only 2-fold slower ligation kinetics. When 1, 2, or 3 nucleotide(s) of the 18 dispensable nucleotides were retained (i.e., only 17, 16, or 15 nucleotides were deleted), the catalytic activity improved and reached 80% of the wt k_{obs} in 20 mM Mn^{2+} for 9F7 min (Figure S9). Importantly, the acceleration of the ligation reaction with Tb^{3+} was as effective for the minimized variant as for the wt (Figure 5 and Figure S10).

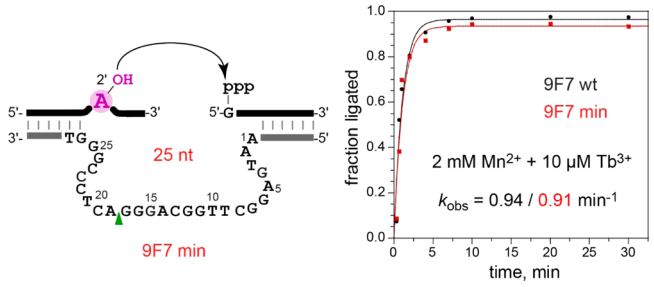

Figure 5. Minimized 9F7 deoxyribozyme and comparison of ligation kinetics of wt and 9F7 min under optimal conditions. The green arrow indicates the deletion of 15 nt with respect to wt. Results for other metal ion combinations in Figure S10.

Careful inspection of the interference results in Figure 4 revealed several other interesting features. First, the 2′-OH group (used as chemical tag for identification of interference effects) had an inhibitory effect at several critical positions, when the ligation reaction was performed with 2 mM Mn^{2+} or 80 mM Mg^{2+}. At low [Mn^{2+}], ribonucleotides were not well tolerated at A1, A2, G4, C8, G12, A14, C38, G39. Strikingly, addition of 10 μM Tb^{3+} to 2 mM Mn^{2+} relieved the 2′-OH interference at all positions (Figure 6). A similar result was obtained when Tb^{3+} was used in the presence of Mg^{2+} (Figure S11), although the 2′-OH effect persisted at A1, A2, and A14, while G39 was not affected in the first place. At 20 mM Mn^{2+}, the 2′-OH group was tolerated at all positions. Although 2′-OH interference effects preclude the interpretation of mutation results at these particular positions, these results hint toward conformational sensitivity of the respective nucleotides. Alterations in ribose pucker and/or steric requirements,

dx.doi.org/10.1021/ja406162z | J. Am. Chem. Soc. 2013, 135, 12839−12848

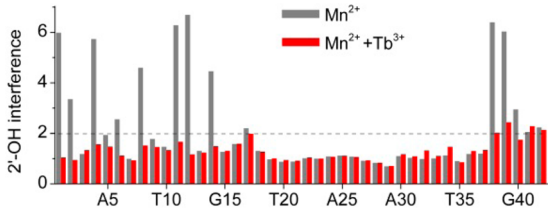

Figure 6. 2′-OH interference values for 2 mM Mn^{2+} (red) and 2 mM Mn^{2+} + 10 μM Tb^{3+} (gray). Analogous data for Mg^{2+} and (Mg^{2+} + Tb^{3+}) in Figure S11.

potentially associated with changes in nucleobase orientation, could negatively impact correct folding of the DNA.

The second group of results concerns the impact of Tb^{3+} on reduced interference values for several mutations. For example, A5G or C13T appeared in the active fractions when Tb^{3+} was present, but the corresponding hydrolysis bands were strongly reduced in the absence of Tb^{3+}. For C38T, this effect was only visible for reactions with Mn^{2+} but not with Mg^{2+}. Several other nucleotides tolerated mutations only with one of the two divalent metal ions (independent of absence or presence of Tb^{3+}), such as A5T and C8G, which showed high interference with Mg^{2+} but lower values with Mn^{2+}. Those nucleotides which cannot be mutated to any other nucleotide under any of the tested conditions are the most critical ones for retaining ligation activity of 9F7, and are found at A1, A2, G4, from G7–G12, and at G39. The CoMA data also revealed nucleotides that tolerated only certain types of mutations, such as only transitions or only transversions. Examples include G15 and G16, at which transversions were tolerated only in the presence of Tb^{3+}, but transitions inhibited activity under all conditions. These mutation results are graphically summarized in Figure S12.

Nucleotides G41 and T42 were included in the mutation analysis as "positive control positions", for which the nucleotide requirements were known from previous studies.[10] These two nucleotides interact with the acceptor substrate upstream of the branch-site nucleotide. Disruption of the DNA–RNA Watson–Crick base pairs inhibited the reaction.[10] The CoMA results confirmed these interactions, since only the parent (ribo)-nucleotides were tolerated, but all mutations showed large interference effects under all assayed conditions. This result supports the interpretation of the interference effects for other nucleotides discussed above.

Tb^{3+} Interactions with the Minimal 9F7 Deoxyribozyme. Having identified a minimal 9F7 deoxyribozyme and potential nucleotide candidates for metal ion interactions by CoMA, we explored sensitized Tb^{3+} luminescence to probe Tb^{3+} interactions with the DNA enzyme and the RNA substrates. To study binding of Tb^{3+} to the deoxyribozyme–substrate complex, we chose a preligation complex formed with inactivated acceptor substrate (**1i**), containing 2′-deoxyadenosine at the branch site. Addition of Tb^{3+} to annealed complexes under various divalent metal ion conditions resulted in an increase in Tb^{3+} luminescence upon excitation at 284 nm. The four distinct emission peaks at 488, 543, 584, and 620 nm (Figure S13) are typical for Tb^{3+} luminescence.[24] Quantitative information on Tb^{3+} binding was obtained by titration experiments up to 200 μM Tb^{3+}, in the presence of 1–100 mM Mg^{2+} or 1–10 mM Mn^{2+}, and measuring the intensity of the corresponding luminescence signal at 543 nm (Figure 7a,b). It is noteworthy that different binding kinetics of Tb^{3+} was

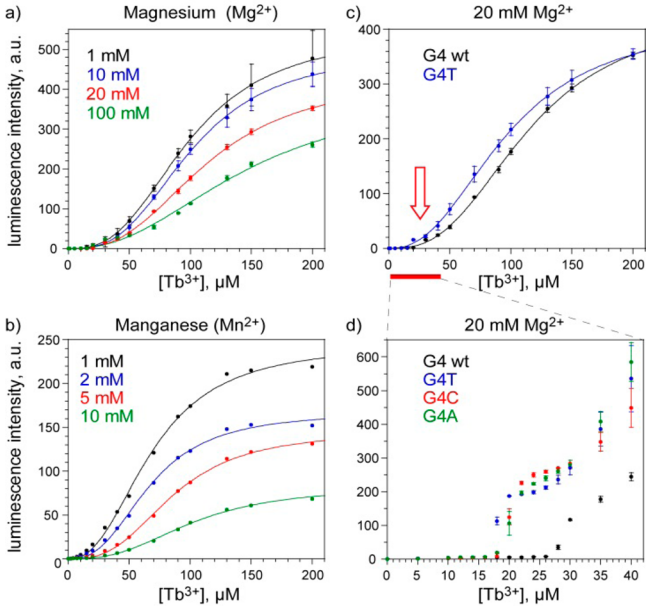

Figure 7. Sensitized Tb^{3+} luminescence. For details see text and Table S3 and Figure S13.

observed depending on type and concentration of the divalent metal ions. In the presence of Mn^{2+}, a fast increase in emission was followed by a slow decrease of characteristic signature within 10 min. In the presence of Mg^{2+}, three different binding modes were observed (Figure S13). At low concentrations of Tb^{3+} (<20 μM), an initial increase was followed by an exponential decay to almost the initial value within 1–3 min. At slightly elevated Tb^{3+} concentrations (between 20 and 60 μM), the signal intensity increased rapidly and stayed at the elevated level for at least 10 min. Higher Tb^{3+} concentrations (>60 μM), resulted in a slower response of the emission intensity. For consistency, the plots in Figure 7 display the emission intensity after an equilibration time of 10 min for each data point. As anticipated for competitive M^{2+} and Tb^{3+} binding, the maximal emission intensities and the apparent affinity for Tb^{3+} (expressed as increasing $[Tb^{3+}]_{1/2}$) decreased with rising divalent ion concentrations. The fit values for binding curves in Figure 7 are summarized in Table S3.

Comparable Tb^{3+} titration experiments were performed with an alternative inactive substrate–enzyme complex that contained a 5′-monophosphate at the donor RNA (**2i**) instead of the reactive triphosphate in **2** (Figure S14). This complex resulted in qualitatively comparable luminescence results as depicted in Figure 7 for the complex with **1i** that lacks the 2′-OH nucleophile, which is a possible site for direct or indirect interaction with metal ions.

Based on the CoMA results, G4 is one potential candidate nucleotide for coordination of metal ions; the sensitivity to the 2′-OH ribose modification is relieved with Tb^{3+}, no mutations are allowed with Mg^{2+}, and a purine nucleotide must be retained for activity with Mn^{2+} (Table S4). A comparison of the luminescene response upon Tb^{3+} titration for 9F7 min (G4 wt) and the inactive G4T mutant in presence of 20 mM Mg^{2+} indicated a slight left-shift of the mutant titration curve upon addition of Tb^{3+} up to 200 μM (Figure 7c). Significant differences were observed at low $[Tb^{3+}]$ (Figure 7d). While a luminescence increase for the wt deoxyribozyme was detected only above 25 μM Tb^{3+}, all three G4 mutants (in which G4 was

dx.doi.org/10.1021/ja406162z | J. Am. Chem. Soc. 2013, 135, 12839–12848

changed to A, C, or T) showed a left-shifted binding curve, indicating facilitated binding of Tb^{3+} when the active site is not intact. These results underline the finding that coordination of a divalent metal ion in the active site is essential for activity and further support the interpretation that Tb^{3+} first binds to peripheral sites before displacing catalytic metal ions and/or causing inactive conformations. However, since the luminescence data were all recorded with inactivated substrates and reported on the sum of specific and unspecific binding of Tb^{3+} to the nucleic acid complex, the luminescence binding curves cannot be directly correlated to the kinetic results.

Although the luminescence data are not sufficient to fully describe all details of Tb^{3+} binding and the mechanism of activation, the results support our kinetic data which suggested that the 9F7 deoxyribozyme provides specific binding sites for Tb^{3+} ions. We hypothesize that acceleration of the ligation activity results from Tb^{3+} binding to structurally important sites which causes an increased affinity for divalent metal ions at catalytically critical M^{2+} binding sites. Studies are underway to gain additional insights into Tb^{3+} coordination from luminescence resonance energy transfer (LRET) using a combination of Tb^{3+} with site-specifically installed fluorescent dyes (e.g., Cy3).[15] In combination with sensitized luminescence, nucleotide analogue interference mapping of DNA (dNAIM)[27] is expected to identify nucleotides that tolerate substitution by 4-thiouridine, known as a good sensitizer for Ln^{3+} luminescence.[35] Luminescence lifetime analyses in water and D_2O as well as Tb^{3+}-induced paramagnetic shifting of ^1H resonances should reveal mechanistic details of Tb^{3+}-assisted acceleration of the 9F7-catalyzed RNA ligation.

Metal-ion mediated folding of the minimized 9F7 deoxyribozyme was further studied by chemical dimethyl sulfate (DMS) probing and enzymatic DNase I footprinting experiments (Figure 8). The accessibility of nucleotides in the catalytic region of 9F7 min was assayed in buffer without divalent metal ions and in the presence of 20 mM Mn^{2+}. Three different sample compositions were used to compare different folding states of the DNA. First, the DNA enzyme was analyzed as the only nucleic acid component in the sample (a, 9F7 min alone), second in complex with inactivated substrates (b, standard acceptor RNA (**1**) and 5′p donor (**2i**)), and third in complex with the 2′,5′-branched RNA product (c). Methylation at N7 of guanosines by DMS, followed by piperidine-mediated cleavage of the DNA backbone at modified positions, reveals the accessibility of the Hoogsteen face of guanosines. For the 9F7 min deoxyribozyme, reduced cleavage intensity was observed for G4, G6, G7, G11, G12, and G15 in the folded DNA–enzyme product complex (c, i.e., in the presence of Mn^{2+}), indicating that these nucleotides are involved in metal ion-dependent tertiary contacts that prevent methylation by DMS. The protection was less pronounced in the more loosely folded sample b (open complex; analysis of cleavage intensities is shown in Figure S15). G16 and G17 remained accessible in all samples, indicating that these nucleotides are not actively participating in formation of the active structure.

Digestion of 9F7 complexes by DNaseI revealed information about the accessibility of the DNA backbone to enzymatic cleavage. DNase footprinting resulted in a strong cleavage band at T20, consistent with the CoMA data that suggested that this nucleotide is not involved in essential interactions or catalysis and is located close to the junction of functionally important regions (note that T20 in 9F7 min corresponds to T35 in 9F7wt, and the dispensable nucleotides were removed between

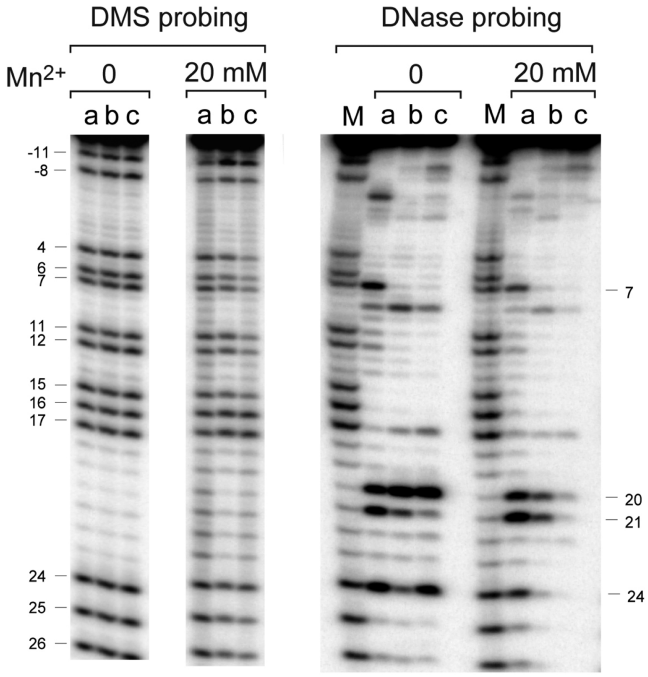

Figure 8. DMS and DNase I probing of 9F7 min. Sample description: (a) 9F7 min alone; (b) 9F7 min deoxyribozyme in complex with (inactive) substrates **1** + **2i** (open complex); (c) 9F7 min deoxyribozyme in complex with 2′,5′-branched RNA product (closed complex). M is the guanosine-specific marker lane.

A18 and C34). Several other positions are also worth highlighting. For example, digestion at G7 was blocked upon hybridization of the binding arms to the RNA substrates/product, even in the absence of Mn^{2+}, while cleavage at position T9 was unaffected. The DNase-mediated strand break at G17 was enhanced in the product–DNA complex, while reduced intensity was observed at C21. Strikingly, cleavage at all DNase-cleavable positions appearing in the absence of Mn^{2+} was strongly diminished in the presence of Mn^{2+}, especially for the folded complex c, although Mn^{2+} is known to increase the activity of DNase I.[18] This observation relates to the metal ion-induced formation of a tight catalytic core that is inaccessible to DNase cleavage. Overall, the footprinting results confirmed the involvement of the critically important guanosine nucleotides in formation of the folded DNA structure.

Tb^{3+}-Mediated Acceleration of RNA Ligation by Other Deoxyribozymes. To investigate the broader applicability of lanthanide-assisted DNA-catalyzed RNA ligation, we studied the effect of Tb^{3+} on the ligation activity of additional deoxyribozymes related to 9F7. The 9F13 DNA enzyme[9] synthesizes 2′,5′-branched RNA also with 5′-triphosphorylated RNA as donor substrate but activates the 2′-OH group of a branch-site uridine instead of adenosine (Figure S16). Tb^{3+} in the presence of 20 mM Mn^{2+} was found to slightly activate the 9F13 DNA-catalyzed reaction at an optimal Tb^{3+} concentration of 10 μM (Figure S17). Higher concentrations up to 50 μM Tb^{3+}caused reduced ligation yields. CoMA of 9F13 revealed numerous nucleotides that were dispensable for activity (Figure S18); the minimized 9F13 variant with 15 nucleotides less in the core region (23 versus 38 nt) ligated the RNA substrates 4-fold faster than the wt sequence (Figure S19). The effect of Tb^{3+} on the minimized 9F13 needs to be further explored to identify the structural features of the DNA core that are

dx.doi.org/10.1021/ja406162z | J. Am. Chem. Soc. 2013, 135, 12839–12848

responsible for activating different nucleophiles (2′-OH on U versus A branch site). Collectively, the results of 9F7 and 9F13 analysis demonstrate that the single-stranded deoxyribozyme core could be reduced to 60−70% of the original length. In both cases, the resulting minimized catalytic sequences contain a high guanosine content of 40−50%.

The 7S11 deoxyribozyme catalyzes the synthesis of 2′,5′-branched RNA in the context of a three-helix junction structure.[8] Upon testing the effect of Tb^{3+} on the ligation kinetics of 7S11, we observed ∼20-fold acceleration with 100 μM Tb^{3+} in the presence of 40 mM Mg^{2+} at pH 7.5. The ligation reaction with 10 mM Mn^{2+} and 10 μM Tb^{3+} was at least 50-fold faster than with Mn^{2+} alone (Figure S20). Higher Tb^{3+} concentrations again caused reduced ligation yields. In contrast to 9F7, 7S11 can use either 5′-triphosphorylated or 5′-adenylated donor substrates, thus offering the possibility to further investigate potential lanthanide coordination to the leaving group. Preliminary results suggest comparable activity with both substrates, indicating that Tb^{3+}-mediated acceleration does not depend on the triphosphate.

Other RNA-ligating deoxyribozymes of practical interest catalyze the linear ligation of donor and acceptor RNA fragments with formation of a native 3′-5′-phosphodiester bond. The best characterized deoxyribozyme of this class is 9DB1, which activates the 3′-OH group of the terminal acceptor nucleotide for nucleophilic attack into the 5′-triphosphate of the donor RNA.[36] Activating cofactors for 9DB1 and its minimized variant[26] were shown to be Mg^{2+} or Mn^{2+}.[36,37] In contrast to the Tb^{3+}-mediated activation of branch-forming deoxyribozymes, the 9DB1-catalyzed linear ligation reaction with Mg^{2+} was not accelerated by the presence of up to 100 μM Tb^{3+} (data not shown). These results indicate that Tb^{3+} acts as a potent cofactor specifically for deoxyribozymes that activate an internal 2′-OH group of a branch-site nucleotide in the acceptor RNA substrate. In contrast, the structural arrangement for DNA-catalyzed activation of the terminal 3′-OH group by 9DB1 is not competent for Tb^{3+}-mediated acceleration.

■ CONCLUSIONS

In this study we have shown that lanthanides act as highly effective cofactors for DNA-catalyzed RNA ligation, thus significantly reducing the concentrations of divalent metal ions required for reaching high rate and yield. For example, with 100 μM Tb^{3+} and 7 mM Mg^{2+}, the 9F7-catalyzed synthesis of 2′,5′-branched RNA was accelerated up to 10 000-fold. The intrinsically faster ligation rates with Mn^{2+} were further increased by the addition of Tb^{3+}. These significant findings open new avenues for creative use of lanthanides in nucleic acid chemistry beyond established functions as structural and mechanistic probing agents and as cofactors for DNA-catalyzed hydrolysis of DNA.[25]

Combinatorial mutation interference analysis under various metal ion conditions guided partial minimization of the DNA catalysts and revealed novel insights into the mutation tolerance of individual nucleotides. We found that the 2′-OH group was better accommodated in the catalytic core of the deoxyribozyme when Tb^{3+} was provided as additional cofactor. The nucleotides at which Tb^{3+} could relieve the 2′-OH effect highlight the importance of the ribose conformation for structure formation and suggest that conformationally sensitive nucleotides may directly interact with metal ions. The mutation interference results also point toward nucleotides involved in tertiary interactions that could be stabilized by metal ions.

Furthermore, we demonstrated that the observed effects of Tb^{3+} acceleration were not restricted to the specific case of 9F7. The related 9F13 deoxyribozyme that uses uridine as branch-site nucleotide (rather than adenosine) was activated by μM concentration of Tb^{3+}. CoMA also guided minimization of 9F13, resulting in a faster variant of the DNA enzyme. In addition, Tb^{3+} accelerated the synthesis of branched RNA in the three-helix junction format of 7S11. The comparison of Tb^{3+}-mediated activation of all studied branched RNA-forming deoxyribozymes revealed an optimal concentration of ca. 100 μM Tb^{3+} in combination with Mg^{2+} but of only 10 μM Tb^{3+} in combination with Mn^{2+}.

Strong concentration dependence and narrow optima for metal ion concentrations have been observed for other DNA enzymes.[38] For example, a DNA-hydrolyzing deoxyribozyme was reported to be most effective with a combination of Zn^{2+} and Mn^{2+} in a precise concentration range,[39] but only two nucleotide mutations enabled the DNA to be active with Zn^{2+} as sole metal ion cofactor.[40] Different types of metal ions can enable catalysis of the same reaction to occur via different mechanisms, as has been proposed for DNA-catalyzed RNA cleavage with Zn^{2+}, Mg^{2+}, or Pb^{2+}, respectively, based on studies of deoxyribozyme folding and catalysis by bulk and single-molecule FRET experiments.[41]

For the deoxyriboyzmes in the center of this study, the structural organization around the active site and the three-dimensional folding of the catalyst are not yet known. Nevertheless, our mutation data, supported by luminescence and footprinting results, suggest interaction networks that will be further refined in combination with future structural data. Recently, the solution structure of a lariat-forming ribozyme (2′-5′ AG1) was solved by NMR, and a model for the active state was built by combining data from mutation analyses and molecular modeling.[42] The 2′-5′ AG1 ribozyme, 9F7, and 7S11 have related substrate requirements (2′-OH at a branch-site adenosine and 5′-triphosphate at guanosine), but the reaction partners are presented in different secondary structure contexts. Future studies will shed light on the question whether similar hypotheses on how metal ions assist ribozyme activity (as derived from NMR structure and modeling) can also be substantiated for DNA-catalyzed synthesis of branched RNA. In this context it is also conceivable that activating metal ions interact simultaneously with the nucleophile and electrophile.

Besides advancing fundamental insights into similarities and/or differences of RNA- and DNA-catalyzed synthesis of 2′,5′-branched RNA, the results of this study have key practical implications. We conclude that the combination of Mg^{2+} or Mn^{2+} with lanthanides, in particular with Tb^{3+}, constitutes a promising approach to drastically enhance the ligation rate and increase the accessibility of RNA structures with branch-site attachments. In this context, the reduced requirement for divalent metal ions in the presence of Tb^{3+} is considered an asset for future applications.

■ EXPERIMENTAL SECTION

Assays of Ligation Kinetics. Standard kinetic assays were performed in a trimolecular format under single-turnover conditions. The 5′-^{32}P trace-labeled acceptor RNA **1** (1 pmol labeled and 4 pmol unlabeled **1**) was annealed with deoxyribozyme (15 pmol) and donor RNA **2** (30 pmol) in 6 μL annealing buffer (5 mM HEPES pH 7.5, 15 mM NaCl, 0.1 mM EDTA) at 95 °C for 2 min, followed by incubation

at room temperature for at least 15 min. The ligation reactions were performed in a volume of 10 μL at 37 °C with a final concentration of 50 mM HEPES pH 7.5, 150 mM NaCl and 2 mM KCl and were initiated by the addition of 1 μL 10× concentrated metal ion stock solution (Mg^{2+} or Mn^{2+} alone or in combination with the respective lanthanides at the indicated concentrations). At appropriate time points, aliquots were quenched into stop solution (80% formamide, 1× TBE [89 mM each Tris and boric acid, pH 8.3], and 50 mM EDTA containing 0.025% bromophenol blue and xylene cyanol). The total reaction times were between 20 min and 24 h. Samples were analyzed by 15% denaturing PAGE and band intensities were quantified using a PhosphorImager. The fractions ligated versus time data were fit to the equation: fraction ligated = $Y\cdot(1 - e^{-kt})$, where $k = k_{obs}$ and Y = final yield.

Combinatorial Mutation Interference Analysis. Combinatorial mutation interference analysis (CoMA) was performed as described earlier.[26] Briefly, mutant libraries were prepared by solid-phase synthesis, radiolabeled at the 3′ end by templated extension with α-^{32}P-dATP using Klenow DNA polymerase, and then ligated to the donor substrate (**2**) using T4 RNA ligase. Separation of active mutants was performed in the presence of 50 mM HEPES pH 7.5, 150 mM NaCl, 2 mM KCl, and 5 different combinations of divalent metal ions (Mg^{2+} or Mn^{2+}) and Tb^{3+} in a volume of 60−70 μL. The reaction times were 20 min for 20 mM Mn^{2+}, 10 h for 2 mM Mn^{2+}, 1 h for 2 mM Mn^{2+} with 10 μM Tb^{3+}, 8 h for 80 mM Mg^{2+}, and 2 h for 80 mM Mg^{2+} with 100 μM Tb^{3+}. Alkaline hydrolysis was performed in presence of 10 mM NaOH by heating at 95 °C for 10 min. Denaturing sequencing gels were run at 35 W for 3−4 h for high resolution. Quantification of interference values was performed by volume or area analysis, as described previously.[26]

Tb^{3+} Luminescence. The inactivated preligation complex was prepared by annealing inactivated acceptor **1a**, 9F7 DNA and donor RNA **2** (1.2 nmol each) in 60 μL in presence of annealing buffer by heating for 2 min at 95 °C and incubation at room temperature for exactly 15 min. Buffer and metal ions were then added to the sample to reach the final concentrations of 2 μM preligation complex, 50 mM HEPES pH 7.5, 150 mM NaCl, 2 mM KCl, and indicated concentration of divalent metal ion in 600 μL. The samples were equilibrated at room temperature for 1 h before Tb^{3+} titration was initiated by addition of small volumes (1 μL) of appropriately concentrated Tb^{3+} stock solution (Figure S5). The luminescence experiments were performed on a Cary Eclipse fluorescence spectrophotometer, with excitation at 284 nm (slit width 10 nm). Emission intensity was collected at 545 nm (slit width: 10 nm; total decay time: 0.02 s; number of flashes: 1; delay time: 0.2 ms; gate time: 5.0 ms). Plots in Figure 7 show luminescence intensities after 10 min equilibration time after addition of each Tb^{3+}-aliquot, plotted as the average of three independent experiments. Data were fit to the equation: $I = I_{max}\cdot[Tb^{3+}]^n/([Tb^{3+}]_{1/2}{}^n + [Tb^{3+}]^n)$.

DMS Probing and DNase I Footprinting. Structural probing experiments were performed with 3′-^{32}P-labeled-DNA. The samples contained DNA alone (a, 0.1 μM), the preligation complex (b, 0.1 μM DNA with 10-fold excess of **1** and **2i**), or the postligation complex (c, 0.1 μM DNA with 10-fold excess of branched RNA product). Samples were incubated at room temperature in the presence of 50 mM HEPES pH 7.5, 150 mM NaCl, 2 mM KCl, and 20 mM $MnCl_2$ (or H_2O) for 5 min in a volume of 10 μL prior to footprinting assays.

Methylation of accessible nucleobases was initiated by adding 1 μL of a freshly prepared solution of 2% DMS in water, followed by incubation at room temperature for 10 min. The reaction was stopped by addition of 1 M β-mercaptoethanol, followed by ethanol precipitation. The pellets were suspended in 50 μL of 10% piperidine, and the DNA was cleaved at the methylated sites upon incubation at 90 °C for 30 min. Piperidine was removed by evaporation under vacuum, and the pellets were washed 2 times with 100 μL 70% ethanol.

DNase I footprinting was performed in presence of 10 mM Tris·HCl pH 7.6, 2.5 mM $MgCl_2$ and 0.5 mM $CaCl_2$ using 0.1 unit DNase I for 10 min at 37 °C. The digestion was stopped by addition of 3 μL of stop solution (80% formamide, 1× TBE, 50 mM EDTA containing 0.025% bromophenol blue and xylene cyanol).

DMS and DNase I samples were separated by denaturing PAGE (20% acrylamide, 1× TBE, 35 W) and analyzed by PhosphorImaging.

■ ASSOCIATED CONTENT

Supporting Information

Figures S1−S20 and Tables S1−S5. This material is available free of charge via the Internet at http://pubs.acs.org.

■ AUTHOR INFORMATION

Corresponding Author

claudia.hoebartner@mpibpc.mpg.de

Notes

The authors declare no competing financial interest.

■ ACKNOWLEDGMENTS

Financial support by the Max Planck Society and the DFG (IRTG 1422, Metal sites in Biomolecules) is gratefully acknowledged. F.J.-Z. was partially supported by a fellowship from the Ph.D. program "Molecular Biology", International Max Planck Research School at the Georg August University Göttingen.

■ REFERENCES

(1) Willner, I.; Shlyahovsky, B.; Zayats, M.; Willner, B. *Chem. Soc. Rev.* **2008**, *37*, 1153.
(2) Silverman, S. K. *Angew. Chem., Int. Ed.* **2010**, *49*, 7180.
(3) Schlosser, K.; Li, Y. *Chem. Biol.* **2009**, *16*, 311.
(4) Höbartner, C.; Pradeepkumar, P. I. In *New strategies in chemical synthesis and catalysis*; Pignataro, B., Ed.; Wiley-VCH, 2012, pp 129−155.
(5) Silverman, S. K.; Baum, D. A. *Methods Enzymol.* **2009**, *469*, 95.
(6) Silverman, S. K. *Acc. Chem. Res.* **2009**, *42*, 1521.
(7) Coppins, R. L.; Silverman, S. K. *Nat. Struct. Mol. Biol.* **2004**, *11*, 270.
(8) Coppins, R. L.; Silverman, S. K. *J. Am. Chem. Soc.* **2005**, *127*, 2900.
(9) Wang, Y.; Silverman, S. K. *J. Am. Chem. Soc.* **2003**, *125*, 6880.
(10) Wang, Y.; Silverman, S. K. *Biochemistry* **2003**, *42*, 15252.
(11) Sigel, R. K. O.; Pyle, A. M. *Chem. Rev.* **2006**, *107*, 97.
(12) Frederiksen, J. K.; Piccirilli, J. A. *Methods* **2009**, *49*, 146.
(13) Sigel, R. K. O.; Pyle, A. M. *Met. Ions Biol. Syst.* **2003**, *40*, 477.
(14) Walter, N. G.; Yang, N.; Burke, J. M. *J. Mol. Biol.* **2000**, *298*, 539.
(15) Yuan, F.; Greenbaum, N. L. *Methods* **2010**, *52*, 173.
(16) Greenbaum, N. L.; Mundoma, C.; Peterman, D. R. *Biochemistry* **2001**, *40*, 1124.
(17) Feig, A. L.; Panek, M.; Horrocks, W. D., Jr.; Uhlenbeck, O. C. *Chem. Biol.* **1999**, *6*, 801.
(18) Cardew, A. S.; Fox, K. R. *Methods Mol. Biol.* **2010**, *613*, 153.
(19) Breaker, R. R.; Joyce, G. F. *Chem. Biol.* **1994**, *1*, 223.
(20) Geyer, C. R.; Sen, D. *J. Mol. Biol.* **1998**, *275*, 483.
(21) Pan, T.; Uhlenbeck, O. C. *Nature* **1992**, *358*, 560.
(22) Ohmichi, T.; Sugimoto, N. *Biochemistry* **1997**, *36*, 3514.
(23) Santoro, S. W.; Joyce, G. F. *Proc. Natl. Acad. Sci. U.S.A.* **1997**, *94*, 4262.
(24) Kim, H. K.; Li, J.; Nagraj, N.; Lu, Y. *Chemistry* **2008**, *14*, 8696.
(25) Dokukin, V.; Silverman, S. K. *Chem. Sci.* **2012**, *3*, 1707.
(26) Wachowius, F.; Javadi-Zarnaghi, F.; Höbartner, C. *Angew. Chem., Int. Ed.* **2010**, *49*, 8504.
(27) Wachowius, F.; Höbartner, C. *J. Am. Chem. Soc.* **2011**, *133*, 14888.
(28) Kim, M. H.; Katahira, M.; Sugiyama, T.; Uesugi, S. *J. Biochem.* **1997**, *122*, 1062.
(29) Erat, M. C.; Sigel, R. K. *Met. Ions Life Sci.* **2011**, *9*, 37.

(30) Takeda, N.; Irisawa, M.; Komiyama, M. *Chem. Commun.* **1994**, *30*, 2773.
(31) Milburn, R. M.; Gautambasak, M.; Tribolet, R.; Sigel, H. *J. Am. Chem. Soc.* **1985**, *107*, 3315.
(32) Forconi, M.; Herschlag, D.; Daniel, H. *Methods Enzymol.* **2009**, *468*, 311.
(33) Piccirilli, J. A.; Vyle, J. S.; Caruthers, M. H.; Cech, T. R. *Nature* **1993**, *361*, 85.
(34) Forconi, M.; Lee, J.; Lee, J. K.; Piccirilli, J. A.; Herschlag, D. *Biochemistry* **2008**, *47*, 6883.
(35) Morrow, J. R.; Andolina, C. M. *Met. Ions Life Sci.* **2012**, *10*, 171.
(36) Purtha, W. E.; Coppins, R. L.; Smalley, M. K.; Silverman, S. K. *J. Am. Chem. Soc.* **2005**, *127*, 13124.
(37) Büttner, L.; Seikowski, J.; Wawrzyniak, K.; Ochmann, A.; Höbartner, C. *Bioorg. Med. Chem.* **2013**, DOI: 10.1016/j.bmc.2013.04.007.
(38) Gu, H.; Furukawa, K.; Weinberg, Z.; Berenson, D. F.; Breaker, R. R. *J. Am. Chem. Soc.* **2013**, *135*, 9121.
(39) Chandra, M.; Sachdeva, A.; Silverman, S. K. *Nat. Chem. Biol.* **2009**, *5*, 718.
(40) Xiao, Y.; Allen, E. C.; Silverman, S. K. *Chem. Commun.* **2011**, *47*, 1749.
(41) Kim, H. K.; Rasnik, I.; Liu, J.; Ha, T.; Lu, Y. *Nat. Chem. Biol.* **2007**, *3*, 763.
(42) Carlomagno, T.; Amata, I.; Codutti, L.; Falb, M.; Fohrer, J.; Masiewicz, P.; Simon, B. *J. Am. Chem. Soc.* **2013**, *135*, 4403.